ICANS-XV
15th Meeting of the International Collaboration on Advanced Neutron Sources
November 6-9, 2000
Tsukuba, Japan

16.6
ON THE ANALYSIS OF DEEP INELASTIC NEUTRON SCATTERING EXPERIMENTS

J. J. Blostein, J. Dawidowski* and J. R. Granada

Comisión Nacional de Energía Atómica and CONICET
Centro Atómico Bariloche and Instituto Balseiro
8400 Bariloche - ARGENTINA
*E-mail: javier@cab.cnea.gov.ar

Abstract

We analyze the different steps that must be followed for data processing in Deep Inelastic Neutron Scattering Experiments. Firstly we discuss to what extent multiple scattering effects can affect the measured peak shape, concluding that an accurate calculation of these effects must be performed to extract the desired effective temperature from the experimental data. We present a Monte Carlo procedure to perform these corrections. Next, we focus our attention on experiments performed on light nuclei. We examine cases in which the desired information is obtained from the observed peak areas, and we analyze the procedure to obtain an effective temperature from the experimental peaks. As a consequence of the results emerging from those cases we trace the limits of validity of the convolution formalism usually employed, and propose a different treatment of the experimental data for this kind of measurements.

1. Introduction

Deep Inelastic Neutron Scattering (DINS), first employed by Hohenberg and Platzman in the study of the Bose condensation in ^{4}He [1], is a technique nowadays widely employed in determining the momentum distributions in the study of the dynamics of atoms in different environments. DINS is a useful tool due to the fundamental information it provides to many fields of Physics, Chemistry and Materials Science. The development of this technique is closely related to the theoretical developments to establish a link between experimental data and the desired momentum distributions, mainly due to Sears [2] and Mayers [3].

DINS experiments, performed in pulsed neutron sources, consist basically in an energy analysis carried out through the use of resonant filters in the range of few eV, either in direct or inverse geometry, the latter being the best one concerning energy resolution [4]. The width of the observed peaks keeps a direct relation with the kinetic energy of each atom, while in other experimental situations the desired information is extracted from the areas of the measured peaks [5]. However, as it will be shown in this paper, the results obtained from this technique, have to be corrected for experimental effects such as attenuation and multiple scattering [6]. Also, an extremely careful treatment must be performed on the experimental

data in order to extract a correct interpretation from them, especially when light nuclei are involved.

2. Basic equations

We will concentrate our analysis on the case of an inverse geometry experiment, i.e. with a resonant filter placed in the path of the neutrons emerging from the sample, which is the most usual configuration [7]. In Fig. 1 we show a schematic diagram of the experiment. Incident neutrons with energy E_0 (characterized by the spectrum $\Phi(E_0)$), travel a distance L_0 from the pulsed source to the sample. After scattering in the sample at an angle θ, neutrons of final energy E travel a distance L_S to the detector position. A resonant filter is placed in the scattered neutron path and consecutive 'filter in' and 'filter out' measurements are performed.

Let $\sigma(E_0,E,\theta)$ be the double differential cross section of the sample which will, hereafter, be considered isotropic. The difference ('filter out' minus 'filter in') in the number of detected neutrons per unit time between times of flight t and $t+\Delta t$ is

$$c(t)\Delta t = \Delta\Omega\Delta t \int_{\substack{E_{inf} \\ t=const.}}^{\infty} dE_0 \Phi(E_0)\sigma(E_0,E,\theta)\varepsilon(E)(1-e^{-nT\sigma_F(E)})\left|\frac{\partial E}{\partial t}\right|, \qquad (1)$$

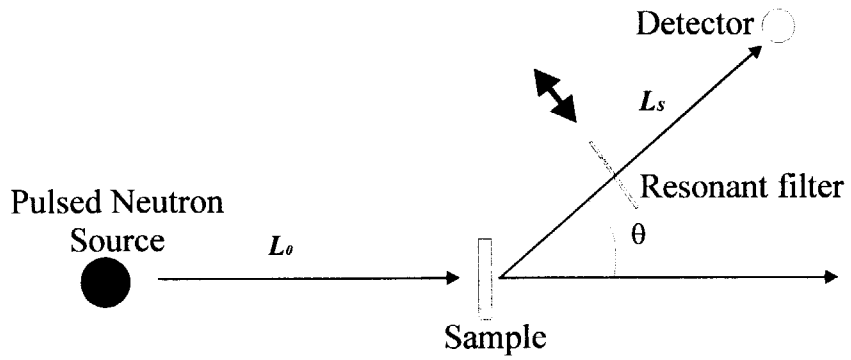

FIGURE 1: Experimental setup

where $\varepsilon(E)$ is the detector efficiency and $\Delta\Omega$ is the differential solid angle subtended by the detector. A filter with a total cross section $\sigma_F(E)$, thickness T, and number density n is interposed in the scattered-neutrons path, the count rate will be affected by the filter transmission. The magnitude expressed in Eq. (1) will be called absorption intensity hereafter, representing the count rate at time t within the channel width Δt.

The total time elapsed since the neutron is emitted from the source until it is detected is

$$t = \sqrt{\frac{m}{2}}\left(\frac{L_0}{\sqrt{E_0}} + \frac{L_S}{\sqrt{E}}\right) \qquad (2)$$

so the integral (1) must be performed at constant time taking into account the relationship (2) between E_0 and E. The Jacobian $|\partial E/\partial t|$ has to be evaluated at a fixed time t according to Eq. (2) as indicated in Ref. [8].

Eq. (1) is the complete description of a neutron Compton-profile as a function of time of flight if only single scattering is considered. An inspection of it reveals that besides the double differential cross section, it depends on the shape of the incident spectrum, the detector efficiency and on the *complete* total cross section of the filter.

3. The convolution approximation

Given that the DINS technique is aimed at obtaining the momentum distribution, the most usual procedure for data treatment is to transform the time scale to the y-scale [3], defined as

$$y = \frac{M}{\hbar^2 q}\left(\hbar\omega - \frac{\hbar^2 q^2}{2M}\right). \tag{3}$$

where M is the mass of the scattering atom, $\hbar q$ is the impulse and $\hbar\omega$ the energy transferred by the neutron to the sample. In this representation, assuming the validity of the Impulse Approximation, it can be shown that the dynamic structure factor $S(q,\omega)$ can be written [2]

$$S(q,\omega) = \frac{M}{\hbar q} J(y). \tag{4}$$

where $J(y)$ is the momentum distribution function along an axis collinear with q.

The usual procedure to relate the experimental time-of-flight measurement with $J(y)$ is to use an **approximate expression** for the absorption intensity instead of Eq. (1) given by [9]

$$c(t)\Delta t = \Phi(E_0)\frac{dE_0}{dt}\Delta t\,\sigma(E_0, E_1, \theta)\varepsilon(E_1)\Delta\Omega\Delta E_1. \tag{5}$$

In Eq. (5) the effect of the filter is expressed by assuming E_1 as the final, well-defined energy of the scattered neutrons, which is the energy of the main absorption peak (4.908 eV in the case of gold). If the sample is assumed to consist of different atomic species, being N_M the number of atoms of mass M and scattering length b_M, the double differential cross section can be expressed, with the help of Eq. (4) as

$$\sigma(E_0, E_1, \theta) = \sum_M N_M b_M^2 \sqrt{\frac{E_1}{E_0}}\frac{M}{q} J_M(y_M) \tag{6}$$

The combined effects of filter resolution and geometric uncertainties are expressed via a mass dependent resolution function $R_M(y_M)$. The final expression in this approximation is then obtained through the convolution

$$c(t)\Delta t = \Phi(E_0)\frac{dE_0}{dt}\varepsilon(E_1)\Delta t\Delta\Omega\Delta E_1\sqrt{\frac{E_1}{E_0}}\frac{1}{q}\sum_M N_M b_M^2 M J_M(y_M) \otimes R_M(y_M). \tag{7}$$

An atom bound in an harmonic potential or free as in an ideal gas presents a gaussian Compton profile $J(y)$, where (the square of) the width is directly proportional to the effective temperature. In the case of an ideal monatomic gas this (square of the) width is directly proportional to the actual temperature. If the scattering system is an atomic gas and its temperature tends to zero, Eq. (7) gives a result proportional to the resolution function, as $J_M(y_M)$ tends to a δ-function in the recoil energy (i.e. $y_M=0$) . This allows to calculate the resolution function for a mass M starting from Eq.(1), where $\sigma(E_0,E,\theta)$ is that of a gas of mass M at zero temperature

A note on the main differences between Eqs. (1) and (7) seems in order. Although both aim at the description of the neutron Compton profile, the first is an essentially exact expression in which for every time of flight all the pairs of compatible energies E_0, E are considered, while in the second the final energy is kept fixed at the filter's resonance value. Furthermore in Eq. (7) a convolution description is imposed, which is not directly deducible from Eq. (1).

4. Analysis of experiments

In this section we will analyze different experimental situations, and we will point out the procedures that have to be followed in order to obtain the desired information from the data.

(a) Multiple Scattering effects

Since the information sought in a DINS experiment is obtained from the peaks' areas and shapes, the first corrections to be undertaken are multiple scattering and

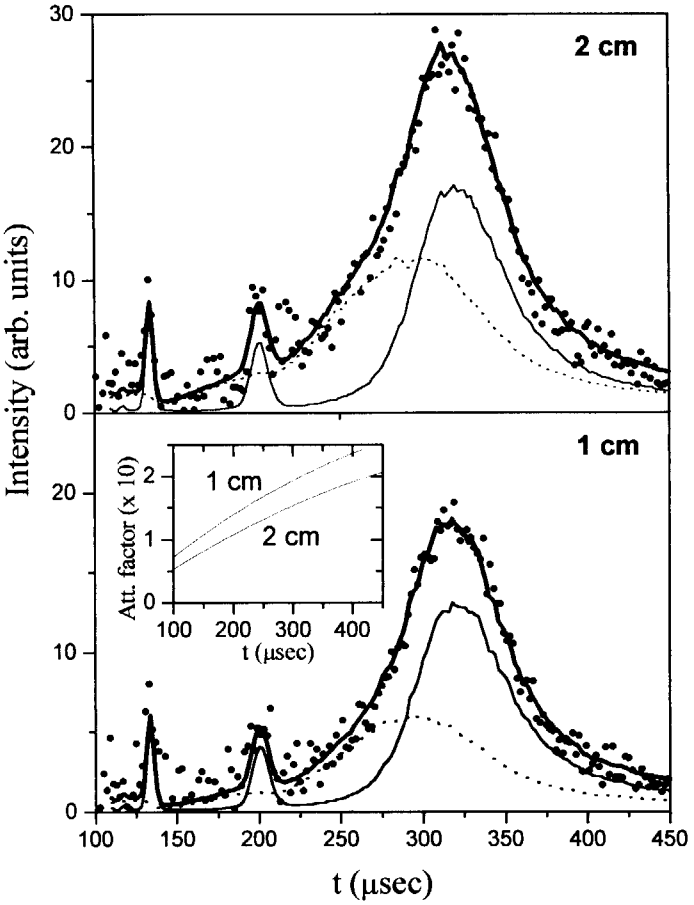

FIGURE 2: DINS profiles for graphite samples with different thicknesses. Experimental data (dots) are compared with Monte Carlo simulations. Single scattering contribution (full thin line), multiple scattering (dotted line), and total scattering (thick line) are shown. Extra peaks at the left are due to additional resonances of Indium. In the inset of the lower frame the attenuation factors of both samples are shown (multiplied by a factor 10).

attenuation effects. To illustrate them we show an experiment performed at the Bariloche electron LINAC (Argentina), on two graphite coin-shaped samples, 3.5-cm diameter and 1 and 2 cm thickness respectively. The sample was placed at 511 cm from the neutron source, and the neutrons were detected at an angle of 56° by six ^{3}He detectors, placed in a hexagonal-corona geometry at 27.5 cm from the sample. The analyzer was an Indium foil 0.19 mm thick. A Monte Carlo code described elsewhere [6] was devised to calculate the multiple scattering and attenuation effects. Fig. 2 illustrates the experimental results along with the results from the numerical simulations. Agreement between both results is very good. A substantial contribution from the multiple-scattering component is apparent for the proposed geometry, and causes an asymmetry towards the lower time-of-flight channels. In the inset of the same figure we show the attenuation factor, which has to be applied to the single scattering data in order to get the proper shape of the single-scattering peak. It is observed that it provides another source of asymmetry.

(b) Peak areas

In all the subsequent analysis, the geometrical parameters to be used are L_0= 1105.5 cm, L_S= 69 cm and θ= 69^0, chosen to match a usual configuration of a typical DINS facility [10]. A thin gold foil is proposed as resonant filter 0.017 mm thick, which gives a parameter nT=0.0001 barn^{-1}. We assume a '*1/E*' behavior for the shape of the incident spectrum, and a '*1/v*' behavior for the detectors' efficiency at those epithermal neutron energies.

In the first experimental situation that we will analyze, the required information is to be obtained from the areas of the observed peaks, which in turn are proportional to the scattering cross sections of the corresponding atoms. This situation corresponds to Ref. [5], where an experiment on different mixtures of light and heavy water at room temperature was performed, with the purpose to observe any anomalous relationship between the fraction of the mixture and the scattering cross sections.

To proceed with the analysis, we calculated the absorption intensity curves for different mixtures of light and heavy water according to the complete calculation given by Eq. (1) and their relative intensities were fitted with the convolution approximation. The double-differential cross sections for hydrogen and deuterium were modeled with a gas scattering law, with an effective temperature calculated from the internal molecular modes employed in the Synthetic Model described in Ref. [11]. The effective temperature is

$$\frac{k_B T_{eff}}{M} = \frac{k_B T}{M_{mol}} + \sum_{\lambda} \frac{E_\lambda}{M_\lambda}, \qquad (8)$$

where k_B is Boltzmann's constant, M_{mol} is the molecular mass, and λ denotes a roto-vibrational mode being E_λ the energy of the mode and M_λ the mass associated to it. With the parameters for light and heavy water from Ref. [11] the resulting effective temperatures (times Boltzmann's constant) are 115.22 meV for H in H_2O and 80.11 meV for D in D_2O. As an example, in the inset of Fig. 3 we show the peaks of hydrogen and deuterium for a mixture with 0.5 concentration of deuterium (x_D). Oxygen contribution is well resolved from these peaks and it will not be considered in the following analysis.

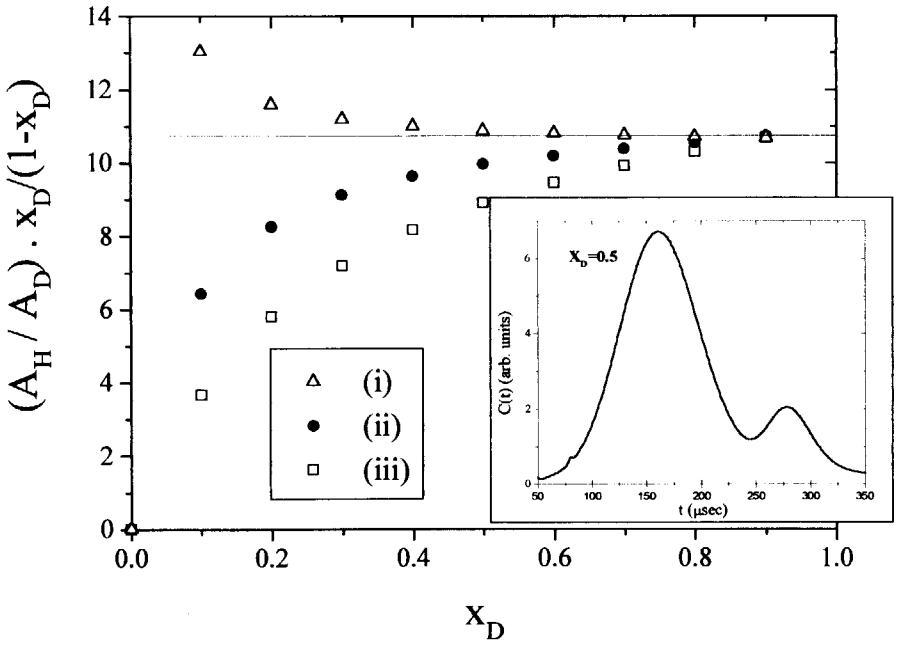

FIGURE 3: Ratio of the fitted areas of the H and D peaks times (x_D/1-x_D) for different resolution functions in several mixtures of light and heavy water. The horizontal line indicates the expected value. In the inset H and D peaks for the mixture x_D=0.5.

Three resolution functions of hydrogen and deuterium obtained in different ways were tested: (i) calculation from a complete description of the total cross section of the gold filter; (ii) the filter cross section is described through a Lorentzian function for the 4.908 eV resonance; (iii) a Lorentzian function in the variable y. In (i) and (ii) the resolution function was obtained as the limit for $T=0K$ of the Compton profiles. Although methods (ii) and (iii) lack a complete description of the filter cross sections, they are the commonly used ones [10].

The magnitude to analyze is the ratio of the intensities of hydrogen to deuterium peaks for a given concentration x_D of heavy water

$$\frac{A_H}{A_D} = \frac{(1-x_D)\sigma_H}{x_D\sigma_D}. \qquad (9)$$

Since σ_H=82.03 barns and σ_D=7.64 barns [12], the quantity $(A_H/A_D)(x_D/1\text{-}x_D)$ must be equal to the constant σ_H/σ_D=10.737. The intensities of the H and D peaks were simultaneously fitted using the convolution approximation, with the three resolution functions mentioned above. A single parameter was fitted for each peak, keeping the effective temperatures fixed for the different mixtures. In Fig.3 we show the ratios of the fitted peak intensities of hydrogen and deuterium times the factor $x_D/(1\text{-}x_D)$ for several mixtures. The overlap between peaks is observed in the inset of the same figure for a particular mixture. With symbols we indicate the results obtained according to different resolution functions in the convolution formalism. A horizontal line indicates the constant value that should be obtained. It is observed that using the full resolution function (above referred as (i)) excess as large as 11% is observed at low x_D, and a consistent value is reached only at large x_D values. The use of resolution function (ii) worsens the discrepancies, (in this case by defect) and reaches 40% of the true value at low x_D, and 65% with the use of resolution function (iii).

Additional information can be added to the problem of area measurements in DINS experiments. According to the exact formulation as well as to the convolution approximation, the peak areas are mass dependent. This dependence is illustrated in Fig. 4, where the areas of different atomic masses ranging from 1 to 12 are compared. The scattering angle in the calculations was 69°, and the effective temperature of the atoms 80 meV.

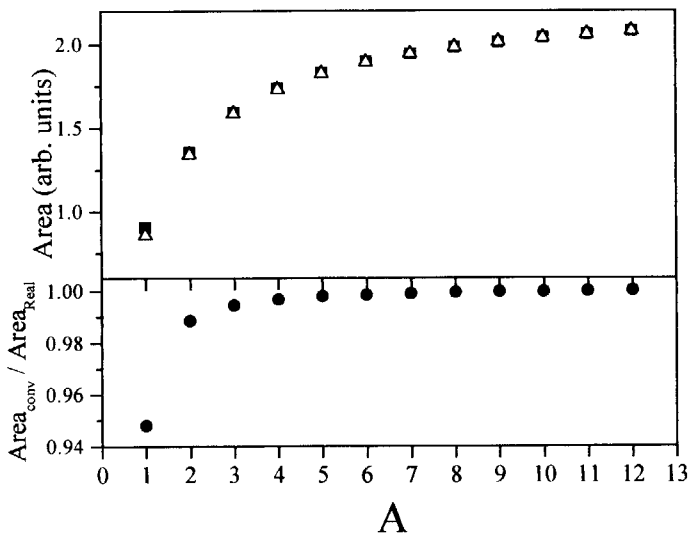

FIGURE 4: Comparison between the areas calculated with the exact formalism (black squares) and the convolution approximation (white triangles). In the lower frame the ratios of both calculations is shown

In the lower frame of Fig. 4 we compare the ratios of both calculations, showing that especially in the case of hydrogen, discrepancies of 5% are obtained if the convolution approximation is used.

(c) Fitting of effective temperatures

The effective temperature, which characterizes the kinetic energy of the atoms, is the data most commonly sought in DINS experiments. This value is obtained by fitting the experimental data with a known distribution, which is Gaussian in the case of an ideal gas or a harmonic oscillator [10].

We will examine the question of extracting the effective temperature in experiments performed on hydrogen, deuterium, ^{3}He and ^{4}He. In the following we will consider that the overlap with other peaks has been properly removed, so we will consider only a single peak. The studied peaks were generated in the time-of-flight scale by means of Eq. (1) with an ideal gas model, with several input temperatures. We then tested the ability of the convolution model, Eq.(7), to fit the generating temperatures, using the resolution functions (i) and (ii) mentioned in the preceding section.

In Fig. 5 we compare the results thus obtained. We will examine firstly the results corresponding to ^{3}He and ^{4}He. It is clearly seen that at low temperatures discrepancies as large as 50% by defect are observed using resolution function (ii) while using resolution function (i) these discrepancies are 20% by excess. At higher effective temperatures the fitted temperatures tend to the same value employing both resolution functions. In the case of H and D the fitted effective temperatures show the same trend as a function of the input temperature, but in H the discrepancies in both resolution functions are relatively small, although the obtained values have systematic errors always by excess.

5. Discussion and conclusions

In this paper we analyzed different situations that arise in DINS experiments, and discussed the different ways to interpret the data, examining the limits in which the usual approaches can lead to wrong results.

We derived Eq. (1), which is the complete description of the observed neutron Compton profile as a function of time of flight. This essentially exact expression contains the detailed shape of the incident spectrum as a function of the neutron energy, the transmission of the analyzer filter and the detector efficiency, and *is not reducible to a convolution form in the variable y*. It is worth to mention that we left aside the geometric effects, that in the case of the convolution formalism, Eq.(7), add a gaussian component to the resolution function, while in the exact formulation it should add extra integrals in the spatial coordinates.

The effect of multiple scattering and attenuation were shown in carbon samples of different sizes. Monte Carlo calculations show good agreement with the experimental results. The effects are important and this stresses the need to carry out good corrections in order to proceed with further analysis. In order to perform these calculations a complete description of the experimental setup has to be included.

In the next example where mixtures of light and heavy water were analyzed, the interest is focussed in the intensities of the observed peaks. Despite the fact that this is not the most usual situation in DINS experiments, it was recently a subject of great interest [5]. In the cited reference an anomalous behavior in the ratio σ_H/σ_D in a DINS experiment was proposed, although those results were not confirmed by high precision neutron interferometric experiments [13]. Similar anomalies are found in our convolution-based analysis, as shown in Fig. 4. A careful analysis indicates that the anomalies emerging from the calculations performed with resolution functions (ii) and (iii) are caused by an incomplete description of the gold filter's total cross section. Notably, they do not properly describe the low-energy '1/v' behavior of the gold filter. This is translated in the negative values of the y-scale, which in turn causes a tail on the right of the H peak (in the time-of-flight scale) not described in the proposed resolution functions, thus resulting in an excess fitted area for the D peak. The net result is an incorrect value for the ratio of the peak areas (Eq. (9)), which worsens with the lower D concentrations due to the considerable overlap between the H and D peaks. We also demonstrated that the mass dependence of the peak areas must correctly be taken into account if conclusions have to be drawn from area measurements. Recent results using this technique ascribe an anomalous behavior in the peak's areas of light nuclei to new phenomena [14].

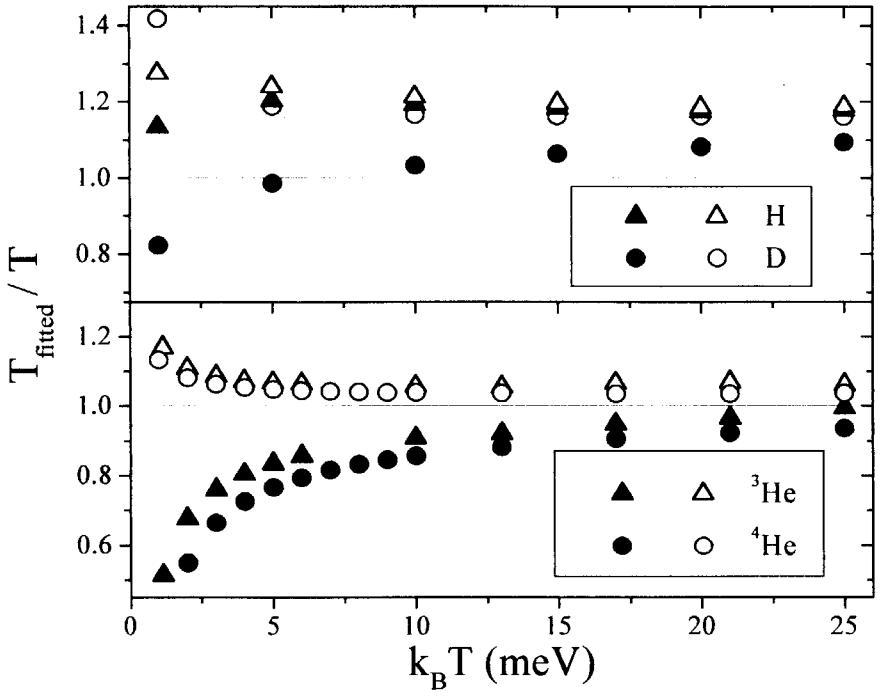

FIGURE 5. Ratio of the fitted temperature to the input temperature for H, D, ^{3}He and ^{4}He at several input temperatures. The input distributions are based on the complete calculation (Eq. (1)), while the fitting models are based on the convolution approximation. Black symbols indicate a fitting model performed with the convolution approximation (resolution function (ii)), while the white symbols use resolution function (i).

Although resolution function (i) is not usually employed a short comment on it seems in order. Despite it takes into account the full cross section of the gold filter, the discrepancies of the obtained results brings out the inadequacy of the convolution formalism to substitute Eq. (1). Two main reasons make this formalism to fail: (a) the peaks in the time of flight scale are not properly centered and, (b) the width of the peaks is underestimated. These facts enhance the defects in the fitted areas, especially in this case where we have considerable overlap between peaks. Also to notice, if we analyze mixtures of hydrogen and deuterium in different environments than the light/heavy- water system, the results should be different from the present ones, given that the different effective temperatures involved may cause different overlap between peaks.

The analysis of the effective temperatures that arises in a DINS experiment produces some interesting results on the way that the data must be processed. Regarding effect (a) mentioned in the previous paragraph, it must be mentioned that the peaks experience a shift towards higher times of flight as the temperature raises. The description of the peak center contained in the approximated Eq. (7) differs from the exact expression, Eq. (1). The convolution formalism overestimates the time shift of the peaks in about 1 μsec for H and D and in a lesser extent for ^{3}He and ^{4}He. It is worth noting that this discrepancy was observed experimentally on hydrogen as shown in Ref. [10]. Also to notice, this time-shift will be lesser for larger masses due to the narrower momentum distributions involved in Eq. (1).

On the other hand, the cause for effect (b) must be found in the fact that the convolution formalism is formulated in the y-variable, and translated to time of flight afterwards. The passage from y to t is made using Eq. (3) where for the calculation of q and ω it was assumed that E_1 is fixed. If the passage from y to t would take into account the finite width of the gold resonance it should be calculated as a convolution between the distribution

in y and a distribution function $f(y,t)$ which would widen the observed distribution in t. The width of that distribution must be compared with the resolution width. It is observed that this uncertainty in the passage from y to t is especially important for $A=1$, thus producing an artificial narrowing in the convolution approximation. Given that the narrowing is caused by the passage from y to t, this effect will be different for the different variables intervening in Eq.(3) (i.e. thickness of the filter, filter type and geometric configurations).

To complete the analysis of the result obtained in Fig. 5, another feature concerning the resolution functions must be taken into consideration. Figure 6 shows the typical full-width-at-half-maximum (FWHM) of the resolution functions of H, D, ^{3}He and ^{4}He compared with the FWHM corresponding to the distribution function $J(y)$ as a function of temperature, whose expression is

$$\Delta J = \sqrt{2\ln 2 \frac{Mk_BT}{\hbar^2}}. \qquad (10)$$

It is seen that for hydrogen, the width of the distribution dominates over the resolution width over all the temperature range shown, except at very low temperatures (below k_BT=1 meV). In the case of deuterium, the convolution is dominated by the resolution function below some 3 meV, 5 meV for ^{3}He and 8 meV for ^{4}He. These limits mark the regions where the largest discrepancies of the fitted temperatures are manifested (see Fig. 5), i.e. in the region dominated by the resolution function. On the other hand, in the regions dominated by the distribution $J(y)$ the fitted temperatures are closer but never equal to the exact value, due to the above mentioned effects (a) and (b). For heavy nuclei, the effect of the resolution function dominates at all temperatures of interest, and this is the reason why lead is commonly used as a callibrator.

It is interesting to comment that in the case of ^{3}He and ^{4}He, the fitted temperatures which are about 50% of the real temperature, in the low temperature region (about 1 meV) proper of the liquid phase have an experimental correlate. DINS experiments reported on Ref. [15] on liquid ^{3}He produced an unexplained fitted value of the effective temperature a factor 2 lower than the theoretical predictions. In the cited paper the convolution formalism was used in the analysis. In the case of ^{4}He no anomalies in the expected value are reported, but the present result should merit a careful revision on those data. It must be emphasized that the discrepancies shown in the present work are referred to the ideal gas model employed to describe all the proposed systems, which clearly does not hold in the case of liquid ^{3}He and ^{4}He. In these cases a better model to quantify the above mentioned discrepancies is imperative. In the case of hydrogen, examples of such unexplained anomalous results can be found in the literature [16] where effective temperature values lower than expected were found for hydrogen in amorphous hydrogenated carbon.

In summary, in the present work we call attention on the usual *modus operandi* employed in the analysis of DINS experiments. The usually employed convolution approximation fails in several aspects:

- Deficient description of the peaks' right tail in the time-of-flight scale using resolution functions (ii) and (iii),
- Position of the peaks' maxima in time-of-flight scale,
- Peaks' areas, especially for light nuclei,
- Observed distribution width.

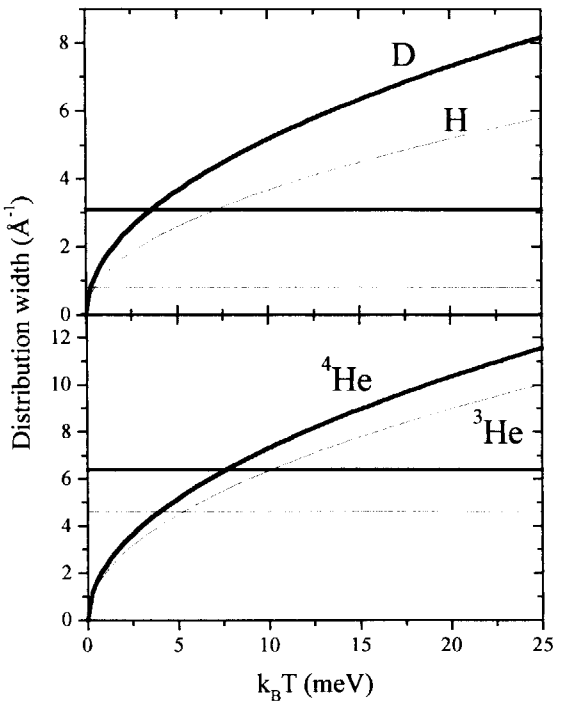

and we have discussed examples where those problems lead to wrong results.

From the present results, we propose that the analysis procedure must be based on the complete expression (Eq.(1)) for the absorption intensity on the time-of-flight scale, after a careful multiple-scattering and attenuation correction is performed. A precise knowledge of the incident spectrum, the detectors' efficiency and the filter total cross section as a function of energy are of primary necessity.

FIGURE 6. FWHM of the resolution function (horizontal line) compared with that of the momentum distribution J(y) as a function of the temperature. Upper frame: H (thin line) and D (thick line). Lower frame: ^{3}He (thin line) and ^{4}He (thick line).

References

[1] P.C. Hohenberg and P.M. Platzman, *Phys. Rev.* **152** , 198 (1966).
[2] V.F. Sears *Phys. Rev.* B **30**, 44 (1984).
[3] J. Mayers, *Phys. Rev.* B **41**, 41 (1990).
[4] R.M. Brugger, A.D. Taylor, C.E. Olsen, J.A. Goldstone and A.K. Soper, *Nucl. Instr. and Meth.* **221**, 393, (1984)
[5] C.A. Chatzidimitriou-Dreismann, T. Abdul Redah, R.M.F. Streffer and J. Mayers, *Phys. Rev. Lett.* **79**, 2839, (1997).
[6] J. Dawidowski, J.J. Blostein and J.R. Granada, *Neutrons and Numerical Methods*, edited by M.R. Johnson, G.J. Kearley and H.G. Büttner, American Inst. of Phys. p.37 (1999)
[7] A.C. Evans, J. Mayers, D.N. Timms and M.J. Cooper, *Z. Naturforsch.* **48a,** 425 (1993).
[8] J.G. Powles, *Mol. Phys.* **26**, 1325 (1973).
[9] C. Windsor, *Pulsed Neutron Scattering,* Taylor and Francis p.366 (1981).
[10] J. Mayers and A.C. Evans, Rutherford Appleton Laboratory report No. RAL-TR-96-067 (1996).
[11] J.R. Granada, *Phys. Rev.* B **31**, 4167, (1985).
[12] L. Koester, H. Rauch and E. Seyman, *Neutron News* **3**, 29 (1992)
[13] A. Ioffe, M. Arif,. D.L. Jacobson and F. Mezei, *Phys. Rev. Lett.* **82**, 2322, (1999).
[14] B. Karlsson, C.A. Chatzidimitriou-Dreismann, T. Abdul-Redah, R.M.F. Streffer, B. Björvarsson, J. Öhrmalm and J. Mayers, *Europhys. Lett.* **46**, 617, (1999); C.A. Chatzidimitriou-Dreismann, T. Abdul-Redah and J. Sperling, *J. Chem. Phys.* **113**, 2784, (2000).
[15] Y. Wang and P.E. Sokol, *Phys. Rev. Lett.* **72**, 1040 (1994).
[16] J. Mayers, T.M. Burke and R.J. Newport, *J. Phys.: Condens. Matter* **6**, 641 (1994).